

Online Calibration of MOSFET On-State Resistance for Precise Current Sensing

Yang Zhang, *Student Member, IEEE*, Regan Zane, *Member, IEEE*, Aleksandar Prodic, *Member, IEEE*, Robert Erickson, *Member, IEEE*, and Dragan Maksimovic, *Member, IEEE*

Abstract—An approach for online current sensing calibration is presented where an auxiliary switch and a precision sense resistor are connected in parallel with a main power switch to achieve accuracy comparable to the sense resistor method, together with the advantage of essentially no additional power loss. The proposed current-sensing circuit and the calibration methods are particularly well suited for digital controller implementations where the required control and calibration functions can be easily accomplished. Experimental results with a digitally controlled 1.5-V 15-A synchronous buck converter demonstrate functionality of the on-line calibration approach, showing a significant improvement in accuracy over voltage sensing across the power MOSFET on-resistance.

Index Terms—Calibration, current sensing, digital control, switching power supplies.

I. INTRODUCTION

SWITCHING power converters require current sensing for a combination of reasons, including:

- 1) current-mode control implementation;
- 2) current sharing among paralleled modules;
- 3) output voltage positioning [as in voltage regulator modules (VRMs)];
- 4) overload protection.

In high-frequency dc–dc switching converters, many current-sensing methods are used, including addition of an accurate sense resistor (RS), sensing of parasitic resistances such as R_{on} of the power MOSFET (RON), inductor series resistance (RL), and PCB trace resistance (RW), and use of a current-sensing power MOSFET “SenseFet” (SFET) or current transformer (CT) [1]–[5]. In low-voltage, high-current point-of-load applications (such as VRMs), “lossless” methods based on existing parasitics such as the RON, RL, or RW are commonly used to achieve high efficiency. However, these lossless current-sensing methods have relatively poor accuracy due to tolerances and temperature variations of the sensing resistance (R_{on} , R_L , or R_w).

Manuscript received June 14, 2004; revised October 21, 2004. This work was supported by Artesyn Technologies through the Colorado Power Electronics Center (CoPEC). Recommended by Associate Editor L. M. Tolbert.

Y. Zhang, R. Zane, R. Erickson, and D. Maksimovic are with the Electronics and Computer Engineering Department, Colorado Power Electronics Center, University of Colorado, Boulder, CO 80309-0425 USA (e-mail: yzhang@colorado.edu; zane@colorado.edu; robert.erickson@colorado.edu; maksimov@colorado.edu).

A. Prodic is with the Electronics and Computer Engineering Department, University of Toronto, Toronto M5S 3G4 ON, Canada (e-mail: prodic@power.ele.utoronto.ca).

Digital Object Identifier 10.1109/LPEL.2004.839635

In this letter, we propose an approach for precise online calibration of low-accuracy current-sensing methods where an accurate sense resistor R_s is switched into the circuit periodically (e.g., every 1000 cycles) for calibration. The approach can be applied to any lossless current-sensing method (such as RON, RL, or RW sensing), or sensorless current estimation [6], and results in the *combined* advantages of the accurate RS method and the lossless sensing techniques [7]. Here, we develop and demonstrate use of the approach for calibration of RON sensing in low-voltage point-of-load dc power supplies based on a synchronous buck converter. Accurate calibration is achieved through an auxiliary current-sensing circuit placed across the synchronous rectifier. Several techniques for improved accuracy are described and experimentally verified on a digitally controlled 1.5 V, 15 A synchronous buck converter. The method is particularly well suited for digital controller implementation where the required control and calibration functions can be easily accomplished.

II. CURRENT-SENSING CIRCUIT WITH ONLINE CALIBRATION

Our approach is based on combining the RS method as a calibration stage together with any of the lossless current sensing approaches. In this section, we describe a combination of the RS and RON methods, as shown in Fig. 1 for a synchronous buck converter with current sensing across the synchronous rectifier. During normal operation, the converter runs in the RON mode with Q_2 on over the time interval $(1 - D)T_s$, while Q_3 is off. In the normal cycle, the sensed voltage V_s is used to measure the inductor current as

$$I_{\text{sense}} = \frac{-V_s}{R_{\text{on}}} \quad (1)$$

where R_{on} is initially estimated from the MOSFET datasheet (or some other best estimate).

The RON approach provides the benefits of no additional components or power loss but results in poor accuracy due to the component tolerances and sensitivity to temperature. We propose to gain the accuracy benefits of a sense resistor while maintaining the RON benefit of no additional power loss by occasionally switching to the auxiliary MOSFET Q_3 for calibration, while the main synchronous rectifier Q_2 is kept off. In a calibration cycle, the inductor current flows through Q_3 and the accurate sense resistor R_s , resulting in a more precise current measurement

$$I_{\text{calib}} = \frac{-V_c}{R_s} \quad (2)$$

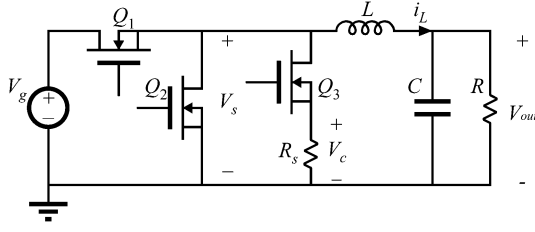


Fig. 1. Synchronous buck converter with current-sensing circuit for online calibration.

The calibration cycle is performed infrequently as required for accurate calibration, allowing a relatively small device Q_3 to be used. Here, we describe three approaches for calibrating R_{on} based on the configuration of Fig. 1.

A. Basic Calibration of Current Sensing

The most straightforward application of (2) is to assume that the inductor current is not affected by the calibration cycle, resulting in a calibrated value of the on-resistance given by

$$R_{on_calib} = R_s \frac{V_s}{V_c}. \quad (3)$$

Then in following normal cycles, this R_{on_calib} is used in (1) instead of the nominal R_{on} to obtain a current sensing accuracy comparable to the RS method. Calibration can be performed infrequently, e.g., every thousands of cycles, to maintain the benefit of lossless RON sensing, while keeping track of slow changes in operating conditions, such as temperature. Note that the approach can calibrate out the effects of temperature variations without sensing the temperature itself, and it can also remove other uncertainties, such as component tolerances and aging. The accuracy of the method depends on the sense resistor R_s , and the assumption that the inductor current is not disturbed during the calibration cycles.

In the circuit of Fig. 1, although the auxiliary switch Q_3 can have a lower current rating compared to the main synchronous rectifier Q_2 , the combined on-resistance of Q_3 and R_s must be low enough so that the body diode of Q_2 is not turned on during calibration cycles. Another practical concern is that a calibration cycle should be performed only when the circuit is operating in steady state, but not in transients. The sensed values of the Q_2 voltage V_s before and after calibration can be used to determine if a large transient has corrupted the calibration measurement.

B. Estimation of the Error Induced in i_L During Calibration

The calibration cycle itself can induce errors in the inductor current due to an increase in the voltage drop across Q_3 and R_s compared to the voltage drop across the main synchronous rectifier Q_2 . This creates a larger inductor voltage during calibration, resulting in an increased current slope as shown in Fig. 2. The induced error can be particularly large in converters (such as VRMs) with low output voltages and low inductance values. This current error i_{L_error} can be estimated from the geometry of

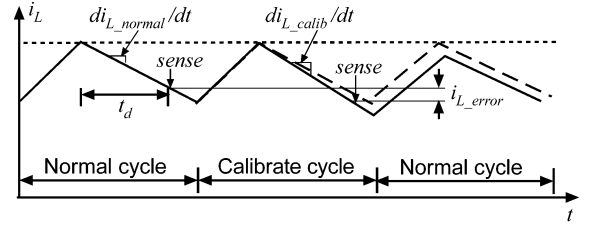


Fig. 2. Error induced in the inductor current during calibration cycles.

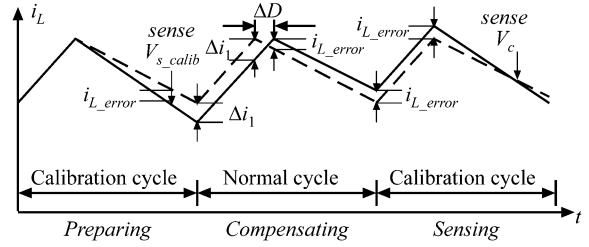


Fig. 3. Active cancellation of the error induced in i_L by injecting ΔD during the compensating cycle to remove i_{L_error} from the V_c measurement in the sensing cycle.

Fig. 2 assuming that the inductance value L and the time delay t_d for sampling are known

$$i_{L_error} = t_d \cdot \left(\frac{(-V_{s_calib}) - (-V_{s_normal})}{L} \right) \quad (4)$$

where V_{s_normal} and V_{s_calib} are the voltages at V_s in Fig. 1 during normal and calibration cycles, respectively. Equation (4) can then be used to cancel the induced current error in the calibration measurement. A modified on-resistance from (3) including a correction factor based on (4) to cancel the current error from the calibrated on-resistance is given by

$$R_{on_calib} = R_s \cdot \frac{V_{s_calib}}{V_c} \cdot \frac{1}{1 + \frac{i_{L_error} \cdot R_s}{-V_c}} \quad (5)$$

resulting in a more accurate I_{sense} when this R_{on_calib} is used in (1) during normal cycles. Additional accuracy can be gained by using multiple samples during the calibration cycle to measure the inductor current slope and actively estimate the inductance value.

The additional costs of implementing (4) and (5) over (3) include sensing V_s and V_c simultaneously during calibration cycles and the added computational requirements in (4) and (5). The approach is well suited for applications with digital control where the additional processing requirements can be provided at minimal cost.

C. Active Cancellation of Error Induced in i_L

The next improvement is to actively remove the error induced by the calibration cycles from the measurement by adjusting the duty cycle. This approach can also be used to actively remove any other perturbations in the waveforms resulting from the calibration cycles. One active cancellation option is a three-cycle calibration sequence. The first cycle is a preparation cycle (Q_3 on, Q_2 off), the second is a compensation cycle (Q_2 on, Q_3 off)

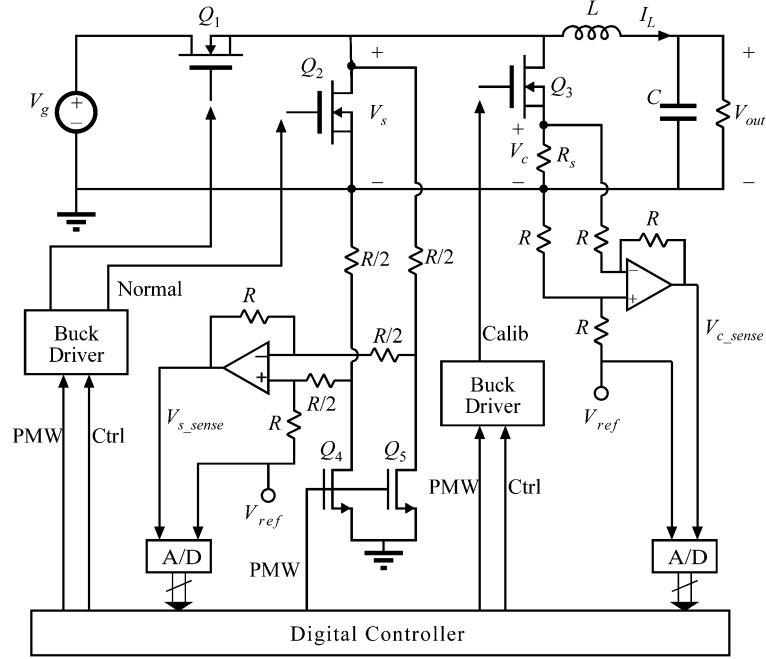


Fig. 4. Experimental test circuit for the online calibrated current sensing method in a synchronous Buck converter.

and the third cycle is the actual sensing cycle (Q_3 on, Q_2 off), as shown in Fig. 3.

In the first cycle, $V_{s_{calib}}$ is sensed to measure the induced current error $i_{L_{error}}$. The purpose of the second cycle (compensating) is to predict and inject a duty cycle change that will force the current at the sensing point of the third cycle to reach the same value that the inductor current has in normal cycles at the time the sampling is performed. Thus the duty cycle is increased by ΔD in the second cycle to compensate for the current error induced in the first and the third calibration cycles. The required change in duty cycle can be derived from the geometry of Fig. 3 and is given by

$$\Delta D = \frac{((-V_{s_{calib}}) - (V_{s_{normal}}))}{V_g} \cdot \left(\frac{t_d}{T_s} + (1 - D) \right). \quad (6)$$

By performing the three-cycle sequence of Fig. 3 based on (6), the V_c measured in the third cycle can be used directly in (3) to calibrate R_{on} since the induced error of (4) has been actively cancelled from the measurement. One key benefit of (6) is that it does not depend on the inductance value, thus having the potential for facilitating very accurate lossless current sensing.

III. EXPERIMENTAL VERIFICATION

An experimental test circuit was built to validate the proposed current sensing and calibration approaches. The test circuit is based on a digitally controlled synchronous buck converter which is employed widely in VRM applications [8], as shown in Fig. 4. The power stage is operating at 100 kHz switching frequency, with 12 V input voltage and 1.5 V output voltage. The load current is between 0 A and 15 A. Two synchronous-buck MOSFET drivers (TPS2838) are used to drive the main control switch Q_1 , the main synchronous rectifier Q_2 , and the auxiliary calibration rectifier Q_3 . The nominal on-resistance for Q_2 is 2.9 m Ω (two Si4888DY MOSFET's in

parallel). The nominal inductance value is $L = 3.0 \mu\text{H}$ and the output capacitance is $C = 750 \mu\text{F}$. The sense resistor is $R_s = 10 \text{ m}\Omega$.

A field programmable gate array (FPGA) based digital controller using a Xilinx Virtex II evaluation board is used to generate the gate-drive signals and to control the current-sampling a/d converters (TI THS1230). Two operational amplifiers (OPA350) and the surrounding circuitry perform differential sensing of V_s and V_c , as well as level shifting of the sensed voltages by V_{ref} . The FPGA takes the outputs of the A/D converters and performs the computations required by (1)–(6). If only the basic calibration method is used, which is described by (1)–(3), one A/D converter can be shared by $V_{s_{sense}}$ and $V_{c_{sense}}$. Note that the calibration methods do not require additional A/D converter resolution over that for normal RON sensing cycles. Thus the A/D resolution is set by the same specifications that motivated current sensing in the converter (e.g., current-mode control, current sharing, protection, or voltage positioning).

In order to test and display alternating normal and calibration cycles easily, the circuit is controlled to have one calibration cycle every three normal cycles. A conversion start signal is also generated for A/D converters to sample and hold V_s and V_c with approximately the same time delay in each cycle. Note that in a practical realization, the calibration cycles would only be performed at a rate based on expected parameter variations (e.g., once per 10 000 cycles or less) so that the added power loss from the calibration cycle would be negligible. In addition, all circuitry associated with calibration can be disabled during normal cycles to avoid any additional power loss over traditional RON sensing.

The basic converter operation is shown in Fig. 5 with the three gate-drive signals and the inductor current waveform when the circuit is operating at full load. Fig. 6 shows the voltage waveforms $V_{s_{sense}}$ and $V_{c_{sense}}$ at the outputs of the differential sensing

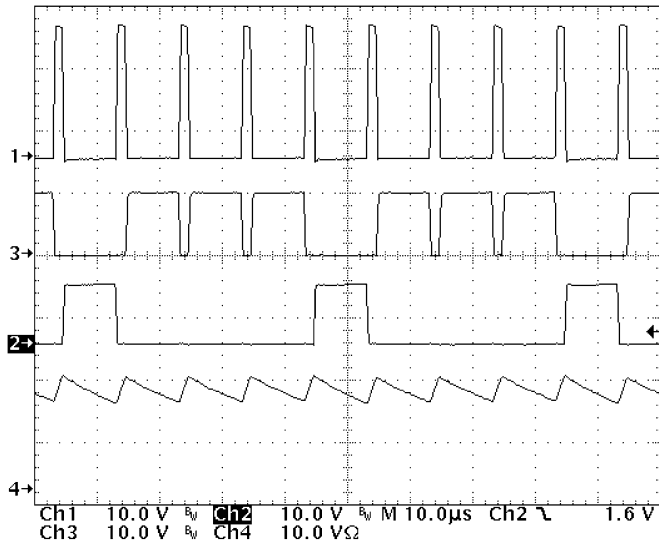


Fig. 5. Top to bottom: the gate drive signal for the main control switch Q_1 ; gate drive signal for the main synchronous rectifier Q_2 ; gate drive signal for the auxiliary calibration rectifier Q_3 and the inductor current i_L at maximum load (15 A).

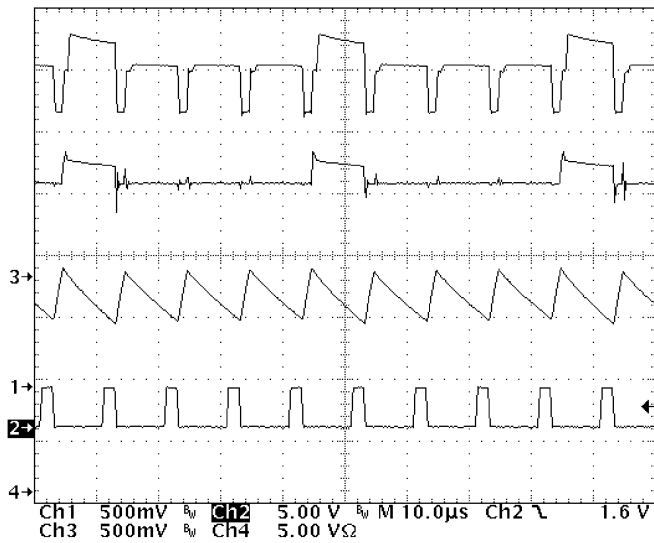


Fig. 6. Top to bottom: $V_{s\text{sense}}$ (Ch.3), $V_{c\text{sense}}$ (Ch.1), the inductor current (Ch.4), and the conversion start signal (Ch.2) at maximum load (15 A).

amplifiers, together with the inductor current and the conversion start signals at full load (15 A). A small disturbance produced by the calibration cycles can be observed in the inductor current waveform.

The experimental results are summarized in Table I at three load levels: 100%, 50%, and 25% of full load. The actual current at the sensing point was recorded and compared to the estimated current based on the RON method alone (without calibration) and with the calibration approaches of Section II. It can be seen that significant improvement is achieved through the basic calibration approach of Section II-A, with additional improvement from the correction in Section II-B at the cost of sampling V_s

TABLE I
EXPERIMENTAL RESULTS FOR ONLINE CALIBRATION

Load (W)	23.6	13.3	6.75
Actual current at sensing point (A)	14.6	8.1	3.8
Percent error (%) in I_{sense} based on (1) with datasheet value for R_{on}	22.8	36.2	45.2
Percent error (%) in I_{sense} using (3) from Section II.A for $R_{\text{on_calib}}$	-2.1	-1.2	-2.6
Percent error (%) in I_{calib} using (5) from Section II.B for $R_{\text{on_calib}}$	0.66	0.96	0.45

and V_c simultaneously during calibration cycles and performing the computations of (4) and (5). Additional accuracy may be required in applications such as VRMs where very low inductance values are used with high currents and the cancellation approach of Section II-C may be required to remove dependence on precise knowledge of the inductance.

IV. CONCLUSIONS

This letter describes an approach for online calibration of current sensing where an auxiliary switch and a precision sense resistor are connected in parallel with a main power switch to achieve accuracy comparable to the sense resistor method, together with the advantage of essentially no additional power loss. The proposed current-sensing circuit and the calibration methods are particularly well suited for digital controller implementations where the required control and calibration functions can be easily accomplished. Experimental results with a digitally controlled 12–1.5 V synchronous buck converter operating at 100-kHz switching frequency demonstrate functionality of the proposed sensing and calibration with a significant improvement in accuracy over voltage sensing across the power MOSFET on-resistance.

REFERENCES

- [1] H. P. Forghani-Zadeh and G. A. Rincón-Mora, "Current-sensing techniques for DC-DC converters," in *Rec., 45th IEEE Midwest Symp. Circuits Systems*, 2002, pp. 577–580.
- [2] E. Dallago, M. Passoni, and G. Sassone, "Lossless current sensing in low-voltage high-current DC/DC modular supplies," *IEEE Trans. Ind. Electron.*, vol. 47, pp. 1249–1252, Dec. 2000.
- [3] D. Grant and R. Williams, "Current sensing MOSFET's for protection and control," *Rec., IEE Colloq. Measurement Techniques Power Electronics*, pp. 8/1–8/5, 1992.
- [4] "Current-sensing power MOSFET's, ON Semiconductor Application Note, Rev.5," ON Semiconductor, AND8093/D, 2002.
- [5] R. Lenk, "Optimum current sensing techniques in CPU converters," Fairchild Semiconductor, Fairchild Application Bulletin AB-20.GI.
- [6] P. Midya, M. Greuel, and P. T. Krein, "Sensorless current mode control—An observer-based technique for DC–DC converters," *IEEE Trans. Power Electron.*, vol. 16, pp. 522–526, Jul. 2001.
- [7] Y. Zhang, R. Zane, D. Maksimovic, and A. Prodic, "On-line calibration of lossless current sensing," in *Rec., IEEE Applied Power Electronics Conf. Exposition*, vol. 2, Feb. 2004, pp. 1345–1350.
- [8] A. V. Peterchev, J. Xiao, and S. R. Sanders, "Architecture and IC implementation of a digital VRM controller," *IEEE Trans. Power Electron.*, vol. 18, pp. 356–364, Jan. 2003.